British Journal of Mathematics & Computer Science
5(2): 133-158, 2015, Article no.BJMCS.2015.011
ISSN: 2231-0851

SCIENCEDOMAIN *international*
www.sciencedomain.org

Simulation of Suspensions of Helical Rigid Fibers

Yazid Al-Hassan[1*]

[1]*Department of Mathematics and Statistics, University of Regina, Canada.*

Article Information

DOI: 10.9734/BJMCS/2015/12581
Editor(s):
(1) Sheng Zhang, Department of Mathematics, Bohai University, China.
Reviewers:
(1) Ette Harrison Etuk, Department of Mathematics/Computer Science, Rivers State University of Science and Technology, Nigeria.
(2) Anonymous, College of Materials Science and Engineering, Qiqihar University, China.
(3) Anonymous, Kolej Matrikulasi Labuan (Kml), Malaysia.
Complete Peer review History: http://www.sciencedomain.org/review-history.php?iid=726&id=6&aid=6659

Original Research Article

Received: 08 July 2014
Accepted: 01 September 2014
Published: 23 October 2014

Abstract

The study at hand presents a numerical method for simulations of the dynamics of slender rigid fibers immersed in an incompressible fluid. The underlying mathematical formulation is based on a slender body approximation as applied to a boundary integral equation for Stokes flow. The curvature and torsion of the fibers can be arbitrarily specified, and we consider fiber shapes ranging from moderately bent to high curvature helical shapes. Two different settings are considered; naturally buoyant fibers in shear flow and heavier fibers sedimenting due to gravity. The dynamics show a very rich behavior, with fiber trajectories that display a very different degree of regularity depending on the initial conditions and fiber shape.

Keywords: Curved rigid fibers, helical rigid fibers, fluid dynamics, slender body theory, sedimentation, shear flow, stokes equations.

1 Introduction

Understanding of translational and rotational motion of immersed fibers is an important concern for many applications, such as pulp and paper industries, biological structures (e.g. D.N.A.) and medical applications. Extensive work has been done in the field of fiber suspension flows.

**Corresponding author: alhassay@uregina.ca;*

Orientation change of fibers in viscous flows was found by Jeffery [1] for the case of slow moving flow past an ellipsoidal body. Gallily and Eisner [2] studied the gravitational deposition of fibers in a constant gradient laminar flow. Gallily and Cohen [3] investigated the inertial collection of fibers by spherical droplets by numerically solving the coupled equations of translation and rotation simultaneously. Foss et al. [4], following the same approach, studied the collection of fibers on spherical collectors in two dimensions. Chen and Yu [5] studied the sedimentation of uncharged and charged fibers in a horizontal circular duct. They presented semiempirical formulas for fiber deposition efficiency.

With the development of computational fluid dynamics, the numerical simulation of fiber migration in a viscous fluid has become an effective tool to study fiber orientation [6,7,8,9], avoiding difficult or impossible theoretical derivations. Sugihara-Seki [9] evaluated the fiber motion in a paraboloidal flow using the finite element method, with results that did not quite agree with Chwang's results [6] because of the bounded wall effect.

Additionally, this work was limited to planar fiber motions and ignored three-dimensional fiber migrations. Feng et al. [8] used the method proposed by Hu et al. [7] to simulate the fiber motion with two-dimensional finite element simulations. Unfortunately, the two-dimensional problem ignores important three-dimensional flow behavior. Zhang et al. [10] presented an approach that addresses the general three-dimensional motion of an axisymmetric fiber with various geometries. Zhang et al [10] demonstrated that fiber shape had a significant impact on the fiber orientation, which would affect the rate of fiber alignment in short-fiber-reinforced composite materials.

Shelley and Ueda [11] developed a method based on the non-local hydrodynamic of the fiber. They studied an extensible fiber in order to simulate a growing liquid crystal. Qi [12] studied flexible fiber in a shear flow at finite Reynolds numbers. A flexible fiber was modeled as a chain of spheres with different stiffness. It was observed that the rotation of a flexible fiber changes from rigid fiber rotation to springy, then the more flexible fiber shows S-turn finally. Tornberg and Shelley [13] employed non-local slender body theory to simulate single and multiple fibers with free ends suspended in a background shear flow.

Our work presents a numerical method for simulations of the dynamics curved rigid fibers immersed in an incompressible fluid. The underlying mathematical formulation is based on a slender body approximation as applied to a boundary integral equation for Stokes flow. We consider different fiber shapes ranging from moderately bent to high curvature helical shapes according to arbitrarily chosen curvature and torsion.

2 Problem Formulation

The flows we are considering are at very low Reynolds numbers, so it is appropriate to consider the Stokes equations. Denote the velocity field by $\mathbf{u}(\mathbf{x})$, the pressure by $p(\mathbf{x})$, and let $\mathbf{f}(\mathbf{x})$ be a force acting on the fluid, where $\mathbf{x} = (x, y, z) \in \mathbb{R}^3$. The Stokes equations read

$$\nabla p - \mu \nabla^2 \mathbf{u} = \mathbf{f}$$
$$\nabla \cdot \mathbf{u} = 0$$

where μ is the viscosity of the fluid.

Assume that we have a fiber in the flow, and let Γ be its surface and $\mathbf{u}_\Gamma$ be its surface velocity. A no-slip condition is enforced on Γ and we require that far away $\mathbf{u}(\mathbf{x})$ is equal to the background velocity $\mathbf{U_0}(\mathbf{x})$, also a solution to the Stokes equations. Thus

$$\mathbf{u} = \mathbf{u}_\Gamma \text{ on } \Gamma$$
$$\mathbf{u} \to \mathbf{U_0} \text{ for } \|\mathbf{x}\| \to \infty.$$

A boundary integral formulation for this problem would end up with an integral equation on the fiber surface [14]. In the case of slender fibers, numerical treatment of this problem would be very expensive [15]. As a remedy, slender-body approximation suggests a reduction by replacing the surface of the fiber with its centerline. This is done using fundamental solutions to Stokes equations.

One such fundamental solution is the ***Stokeslet***. If $\mathbf{f} = \delta(\mathbf{x} - \mathbf{x}')\mathbf{e}_i$, where is $\mathbf{e}_i$ the unit vector in direction i, $\mathbf{x}$ is an observation point, $\mathbf{x}'$ is the source point and δ is the three-dimensional delta function, then $\mathbf{u}(\mathbf{x}) = \boldsymbol{\mathcal{G}}(\mathbf{x} - \mathbf{x}')\mathbf{e}_i$ is a solution to the Stokes equations, with the Stokeslet tensor given by

$$\boldsymbol{\mathcal{G}}(\mathbf{R}) = \frac{\mathbf{I} + \hat{\mathbf{R}}\hat{\mathbf{R}}}{|\mathbf{R}|}$$

where $\mathbf{I}$ is the identity tensor, $\mathbf{R} = \mathbf{x} - \mathbf{x}'$ and $\hat{\mathbf{R}} = \mathbf{R}/|\mathbf{R}|$ is a unit vector.

Another fundamental solution, so-called ***doublet***, can be obtained by differentiating the Stokeslet with respect to the source point $\mathbf{x}'$. The doublet is defined as

$$\boldsymbol{\mathcal{G}}_{\boldsymbol{D}}(\mathbf{R}) = \frac{\mathbf{I} - 3\hat{\mathbf{R}}\hat{\mathbf{R}}}{|\mathbf{R}|^3}$$

2.1 The Slender-Body Integral Equations

In slender-body theory the solution is found by matching an inner solution for radial distances much less than the fiber length to an outer solution value at radial distances much greater than the fiber radius, with the inner solution satisfying the no-slip boundary condition on the fiber surface and the outer solution satisfying the condition at infinity [16,17].

Let the centerline of each fiber be parameterized by arc length $s \in [0, L]$, where L is the fiber's length, and let $\mathbf{x}(s,t) = (x(s,t), y(s,t), z(s,t))$ be the coordinates of the fiber centerline. Assuming that the fiber does not reapproach itself, and the radius of the fiber is given by $a(s) = 2\varepsilon\sqrt{s(L-s)}$, where $\varepsilon = \frac{a}{L}$ is the aspect, a slender body approximation of the velocity of the fiber centerline is given by [17]

$$8\pi\mu(\mathbf{u}(\mathbf{x}(s,t),t) - \mathbf{U_0}(\mathbf{x}(s,t),t)) = -\boldsymbol{\Lambda}[\mathbf{f}](s) - \mathbf{K}[\mathbf{f}](s) \tag{0.1}$$

where $\mathbf{f}$ is the force per unit length on the fiber. The local operator $\boldsymbol{\Lambda}[\mathbf{f}](s)$ is given by

$$\Lambda[\mathrm{f}](\mathrm{s}) = \big[-\mathrm{c}\big(\mathrm{I} + \mathrm{TT}(\mathrm{s})\big) + 2\big(\mathrm{I} - \mathrm{TT}(\mathrm{s})\big)\big]\mathrm{f}(\mathrm{s}), \tag{0.2}$$

and the integral operator $\mathbf{K}[\mathbf{f}](s)$ is given by

$$\mathrm{K[f](s)} = \int_0^{\mathrm{L}} \left(\frac{\mathrm{I} + \hat{\mathrm{R}}(\mathrm{s},\mathrm{s}')\hat{\mathrm{R}}(\mathrm{s},\mathrm{s}')}{|\mathrm{R}|}\mathrm{f(s}') - \frac{\mathrm{I} + \mathrm{T(s)T(s)}}{|\mathrm{s}-\mathrm{s}'|}\mathrm{f(s)} \right) \mathrm{ds}'. \tag{0.3}$$

Here $\mathbf{R} = \mathbf{x}(s) - \mathbf{x}(s')$, $\widehat{\mathbf{R}} = \mathbf{R}/|\mathbf{R}|$ and $\mathbf{T}$ is the tangent vector defined. And $\widehat{\mathbf{R}}\widehat{\mathbf{R}}$ and $\mathbf{TT}$ are dyadic products, i.e. $\left(\widehat{\mathbf{R}}\widehat{\mathbf{R}}\right)_{ij} = \widehat{\mathbf{R}}_i\widehat{\mathbf{R}}_j$. The constant $c = \log(\varepsilon^2)$, $c < 0$.

The operator $\mathbf{K}[\mathbf{f}]\ (s)$ is a so-called finite part integral as each term in the integrand is singular at $s' = s$, and the integral is only well defined when the integrand is kept as the difference of its two terms. Note that the operators $\mathbf{\Lambda}[\mathbf{f}](s)$ and $\mathbf{K}[\mathbf{f}]\ (s)$ both depend on the shape of the fiber, as given by $\mathbf{x}(s,t)$. The asymptotic accuracy of Eq. (0.1) is $O(\varepsilon^2\log(\varepsilon))$.

The immersed rigid fiber performs a rigid body motion, in this situation the velocity of the fiber is given by the formula [18]

$$\mathbf{u}\big(\mathbf{x}(s,t)\big) = \mathbf{V} + \mathbf{\Omega} \times (\mathbf{x}(s,t) - \mathbf{x}_c)\ ,\ \ \mathbf{x} \in \Gamma \tag{0.4}$$

where $\mathbf{x}_c$ is the center of mass (the centriod in case of the centerline), $\mathbf{V} = (V_x, V_y, V_z)$ is the translational velocity and $\mathbf{\Omega} = (\omega_x, \omega_y, \omega_z)$ is the rotational velocity. Then Eq. (0.1) can be rewritten as

$$8\pi\mu \left(\mathbf{V} + \mathbf{\Omega} \times (\mathbf{x}(s,t) - \mathbf{x}_c) - \mathbf{U}_0\big(\mathbf{x}(s,t)\big) \right) = -\big(\mathbf{\Lambda}[\mathbf{f}\,](s) + \mathbf{K}[\mathbf{f}\,](s)\big)\,, s\epsilon[0,L] \tag{0.5}$$

To close this system of equations we need to impose the constraints that the integrated force and torque over the fiber equal to the externally applied force and torque, i.e.

$$\int_0^L \mathbf{f}(s)ds = \mathbf{F}_g\,, \qquad \int_0^L (\mathbf{x} - \mathbf{x}_c) \times \mathbf{f}(s)ds = \mathbf{L} \tag{0.6}$$

The system of equations (0.5)-(0.6) is solved for velocities $\mathbf{V}$ and $\mathbf{\Omega}$, and the force $\mathbf{f}$. In the case that there is a density difference $\Delta\rho$ between the fiber and the surrounding fluid, $\mathbf{F}_g = \frac{\Delta\rho g v}{L}\mathbf{e}_g$, where g is the gravitational acceleration and v is the volume of the fiber, assuming that the gravity is acting in direction of $\mathbf{e}_g$. If we consider the case of naturally buoyant fibers, as is of interest for example for fibers in shear flow, then simply $\mathbf{F}_g = \mathbf{0}$. In both cases $\mathbf{L} = \mathbf{0}$, since there is no externally applied torque.

To evaluate the rigid fiber rotation, we define an orthonormal frame $\{\mathbf{T}, \mathbf{N}, \mathbf{B}\}$ fixed to the fiber and update the frame together with the location of the center of mass [19,10], i.e.

$$\dot{\mathbf{x}}_\mathbf{c} = \mathbf{V}, \tag{0.7}$$

$$\dot{\mathbf{Q}} = \mathbf{\Omega} \times \mathbf{Q} \tag{0.8}$$

where $\mathbf{Q} = (\mathbf{T}\ \mathbf{N}\ \mathbf{B})^T$. Eq. (0.8) can be written as

$$\dot{\mathrm{Q}} = \mathrm{BQ} \tag{0.9}$$

where $B = \begin{pmatrix} 0 & -\omega_z & \omega_y \\ \omega_z & 0 & -\omega_x \\ -\omega_y & \omega_x & 0 \end{pmatrix}$.

2.2 Non-Dimensionalization

2.2.1 Shear flow

Assuming $\mathbf{U}_0(\mathbf{x})$ to be a shear flow of a shear rate $\dot{\gamma}$, we non-dimensionalize Eq. (0.1) by introducing the following characteristic parameters:

characteristic length: $L_C = L$
characteristic time: $t_C = 8\pi/\dot{\gamma}$
characteristic velocity: $U_C = \dot{\gamma}L$
characteristic force: $f_C = 8\pi\mu L\dot{\gamma}$

Then we define the dimensionless variables $\mathbf{x}^* = \mathbf{x}/L_C$, $\mathbf{u}^* = \mathbf{u}/U_c$, $t^* = t/t_C$ and $\mathbf{f}^* = \mathbf{f}/f_C$. Substituting these variables in Eqs. (0.1) and (0.6), we obtain

$$(\mathbf{u}^*(\mathbf{x}^*) - \mathbf{U}_0^*(\mathbf{x}^*)) = -(\mathbf{\Lambda}[\mathbf{f}^*](s) + \mathbf{K}[\mathbf{f}^*](s)) \tag{0.10}$$

Now, dropping all * superscripts, we get with the non-dimensional version of Eq. (0.1)

$$\big(\mathbf{u}(\mathbf{x}(s,t)) - \mathbf{U}_0(\mathbf{x}(s,t))\big) = -\big(\mathbf{\Lambda}[\mathbf{f}\,](s) + \mathbf{K}[\mathbf{f}\,](s)\big), s\epsilon[0,1] \tag{0.11}$$

And

$$\int_0^1 \mathbf{f}(s)ds = 0\,, \qquad \int_0^1 (\mathbf{x} - \mathbf{x}_c) \times \mathbf{f}(s)ds = 0 \tag{0.12}$$

such that $s \in [0,1]$. Thus, Eq. (0.11) is controlled only by the parameter $c = \log(\varepsilon^2)$ that appears in the definition of $\mathbf{\Lambda}[\mathbf{f}\,]$ in (0.2).

2.2.2 Sedimentation due to gravity

To non-dimensionalize Eq. (0.1) in the presence of gravitational forces, we use the following characteristic parameters:

characteristic length: $L_C = L$
characteristic time $t_C = \frac{8\pi\mu L^2}{\Delta\rho g v}$
characteristic velocity: $U_C = \frac{\Delta\rho g v}{8\pi\mu L}$
characteristic force: $f_C = \frac{\Delta\rho g v}{L}$

Similar to the shear flow case, we define the dimensionless variables $\mathbf{x}^* = \mathbf{x}/L_C$, $\mathbf{u}^* = \mathbf{u}/U_C$, $t^* = t/t_C$ and $\mathbf{f}^* = \mathbf{f}/f_C$. Substituting these variables in Eqs. (0.1) and (0.6) and dropping all * superscripts, we get with the same dimensionless equation as in(0.11), and

$$\int_0^1 \mathbf{f}(s)ds = \mathbf{e}_g\,, \qquad \int_0^1 (\mathbf{x}-\mathbf{x}_c)\times\mathbf{f}(s)ds = 0 \tag{0.13}$$

such that $s \in [0,1]$, where gravity is acting in the direction of $\mathbf{e}_g$.

2.3 Regularization of K[f]

Each term in the integral kernel of **K[f]** (*see* Eq. (0.3)) is singular at $s' = s$, and the integral is only well defined when the integral kernel is kept as the difference of its two terms. To overcome this problem, we introduce a regularized integral operator $\mathbf{K}_\delta[\mathbf{f}\,]$, defined as

$$\mathbf{K}_\delta[\mathbf{f}\,](s) = \int_0^1 \left(\frac{\mathbf{I}+\widehat{\mathbf{R}}(s,s')\widehat{\mathbf{R}}(s,s')}{\sqrt{|\mathbf{R}(s,s')|^2+\delta^2}}\mathbf{f}(s') - \frac{\mathbf{I}+\mathbf{T}(s)\mathbf{T}(s)}{\sqrt{|s-s'|^2+\delta^2}}\mathbf{f}(s) \right) ds'. \tag{0.14}$$

where $\delta \in \mathbb{R}$.

Tornberg and Shelley [13] defined δ as a function of s such that $\delta(s) = \delta_0\varphi(s)$, where $\delta_0 = m\varepsilon$, $m > \sqrt{2}$, and $\varphi(s) \in C^1(s)$ is given by

$$\varphi(s) = \begin{cases} w(s/\gamma), & 0 \le s < \gamma \\ 1, & \gamma \le s \le 1-\gamma \\ w((1-s)/\gamma), & 1-\gamma < s \le 1 \end{cases} \tag{0.15}$$

where $w(\vartheta) = \vartheta^2(3-2\vartheta)$.

The regularized integral in Eq. (0.14) differs by $O(\delta_0^2 \log\delta)$ to the unregularized one (for the proof see [13], p 35).

2.4 Multiple Fibers

In the case of multiple fibers, we introduce an indexing and denote the fibers by Γ_n, $n = 1, \dots, N$, and the coordinates of the fiber centerline by $\mathbf{x}_n(s,t) = (x_n(s,t), y_n(s,t), z_n(s,t))$. For fiber Γ_n, we have [17].

$$8\pi\mu\big(\mathbf{u}(\mathbf{x}_n(s,t),t) - \mathbf{U_0}(\mathbf{x}_n(s,t),t)\big) = -\mathbf{\Lambda}_n[\mathbf{f}_n](s) - \mathbf{K}_n[\mathbf{f}_n](s) + \sum_{\substack{l=1 \\ l\neq n}}^{N} \int_{\Gamma_l} \mathbf{G}(\mathbf{R}_l)\mathbf{f}_l(s')ds' \tag{0.16}$$

where $\mathbf{R}_l(s,s') = \mathbf{x}_n(s,t) - \mathbf{x}_l(s',t)$; $\widehat{\mathbf{R}}_l = \mathbf{R}_l/|\mathbf{R}_l|$. The sum over $\int_{\Gamma_l} \mathbf{G}(\mathbf{R}_l)\mathbf{f}_l(s')ds'$ represents the contribution from all other fiber to the velocity of fiber n, and $\mathbf{G}(\mathbf{R}_l)$ is given by the

sum of a Stokeslet and a doublet,

$$\mathbf{G}(\mathbf{R}_l) = \frac{\mathbf{I} + \widehat{\mathbf{R}}_l\widehat{\mathbf{R}}_l}{|\mathbf{R}_l|} + a^2\frac{\mathbf{I} - 3\widehat{\mathbf{R}}_l\widehat{\mathbf{R}}_l}{|\mathbf{R}_l|^3} \tag{0.17}$$

where a is the fiber's radius. Similar to equations (0.2) and (0.3), the operators $\mathbf{\Lambda}_n[\mathbf{f}_n](s)$ and $\mathbf{K}_n[\mathbf{f}_n](s)$ are given by

$$\mathbf{\Lambda}_n[\mathbf{f}_n](s) = \left[-c\big(\mathbf{I} + \mathbf{T}_n\mathbf{T}_n(s)\big) + 2\big(\mathbf{I} - \mathbf{T}_n\mathbf{T}_n(s)\big)\right]\mathbf{f}_n(s), \tag{0.18}$$

And

$$\mathbf{K}_n[\mathbf{f}_n](s) = \int_{\Gamma_n}\left(\frac{\mathbf{I} + \widehat{\mathbf{R}}_n(s,s')\widehat{\mathbf{R}}_n(s,s')}{|\mathbf{R}_n|}\mathbf{f}_n(s') - \frac{\mathbf{I} + \mathbf{T}_n(s)\mathbf{T}_n(s)}{|s-s'|}\mathbf{f}_n(s)\right)ds' \tag{0.19}$$

Here $\mathbf{R}_n(s,s') = \mathbf{x}_n(s) - \mathbf{x}_n(s')$, $\widehat{\mathbf{R}}_n = \mathbf{R}_n/|\mathbf{R}_n|$ and $\mathbf{T}_n$ is the tangent vector of the centerline of fiber n.

The dimensionless version of Eq. (0.16) for a shear flow can be written as

$$\Big(\mathbf{u}\big(\mathbf{x}_n(s,t)\big) - \mathbf{U_0}\big(\mathbf{x}_n(s,t)\big)\Big) = -\mathbf{\Lambda}_n[\mathbf{f}_n](s) - \mathbf{K}_n[\mathbf{f}_n](s) + \sum_{\substack{l=1\\ l\neq n}}^{N}\int_0^1 \mathbf{G}(\mathbf{R}_l)\mathbf{f}_l(s')ds' \tag{0.20}$$

$s\epsilon[0,1]$, where $\mathbf{u}(\mathbf{x}_n) = \mathbf{V}_n + \mathbf{\Omega}_n \times \big(\mathbf{x}_n - \mathbf{x}_{n_c}\big)$, $\mathbf{V}_n$ and $\mathbf{\Omega}_n$ are the translational and rotational velocities, respectively, of fiber Γ_n, and $\mathbf{x}_{n_c}$ is the centriod of the centerline of Γ_n.

In order to close this system of equations we need to impose the constraints that the integrated force and torque over each fiber equal to the externally applied force and torque, i.e.

$$\int_0^1 \mathbf{f}_n(s)ds = 0\,, \qquad \int_0^1 \big(\mathbf{x}_n - \mathbf{x}_{n_c}\big) \times \mathbf{f}_n(s)ds = \mathbf{0} \tag{0.21}$$

3 Numerical Treatment

To define an instantaneous position of the immersed fiber, we need only to update the reference point, $\mathbf{x}_c$, and the orientation (i.e., tangent) vector $\mathbf{T}$. First the translational and rotational velocities, **V** and **Ω,** have to be determined by solving the dimensionless versions of Eqs. (0.5) and (0.6). Then the reference point and the orientation can be updated using Eqs (0.7) and (0.8).

3.1 Updating the Fiber Position

To update the position of the fiber, Eqs. (0.7) and (0.8) must be discretized in time. A forward time scheme can be used for this purpose since there are no terms in the equations that impose a strict stability restriction. We have used the *Adams-Bashforth 2-step method* which is an explicit second order multi-step method.

Starting with $t_0 = 0$, let the time step $\Delta t = t_q - t_{q-1}$ where $t_q = q\Delta t$, $q = 0,1,\ldots$. And denote $\mathbf{x}^q$ the numerical approximation of $\mathbf{x}\left(t_q\right)$. Then the discretization of Eqs. (0.7) and (0.8) can be written as

$$\mathbf{x}^{q+1} = \mathbf{x}^q + \frac{\Delta t}{2}(3\mathbf{V}^q - \mathbf{V}^{q-1}) \ , q = 1,2,\ldots \tag{0.22}$$

and

$$\mathbf{Q}^{q+1} = e^{\frac{\Delta t}{2}(3B^q - B^{q-1})}\mathbf{Q}^i \quad , q = 1,2,\ldots \tag{0.23}$$

where $B^q = \begin{pmatrix} 0 & -\omega_z(t_q) & \omega_y(t_q) \\ \omega_z(t_q) & 0 & -\omega_x(t_q) \\ -\omega_y(t_q) & \omega_x(t_q) & 0 \end{pmatrix}$.

The discretization (0.23) yields a method where the triplet of vectors $(\mathbf{T}, \mathbf{N}, \mathbf{B})$ remains an orthonormal frame up to round-off errors. In the first time step, $\mathbf{x}^1$ and $\mathbf{Q}^1$ are computed with the first order forward Euler method.

3.2 Discretization of the Integral Equation

In this section we introduce the discretization of the dimensionless integral equations (0.11) and (0.12) for a shear flow. Similar discretization can be done in the presence of gravitational forces. First we rewrite Eq. (0.11) using the regularized integrand $\mathbf{K}_\delta[\mathbf{f}\,]$ as

$$\begin{gathered} \mathbf{V} + \boldsymbol{\Omega} \times (\mathbf{x}(s,t) - \mathbf{x}_c) + \boldsymbol{\Lambda}[\mathbf{f}\,](s) + \mathbf{K}_\delta[\mathbf{f}\,](s) = \mathbf{U}_0\big(\mathbf{x}(s)\big) \\ \int_0^1 \mathbf{f}(s)ds = 0\,, \qquad \int_0^1 (\mathbf{x} - \mathbf{x}_c) \times \mathbf{f}(s)ds = 0 \end{gathered} \tag{0.24}$$

The centerline $\mathbf{x}(s,t)$ will change with time. At each instant in time, we need to solve (0.24). Dropping the index notation with respect to time, we denote $\mathbf{x}_i = \mathbf{x}(s_i)$ and $\mathbf{f}_i = \mathbf{f}(s_i)$. Then the discretized version of Eq. (0.24) can be written as

$$\begin{gathered} \mathbf{V} + \boldsymbol{\Omega} \times (\mathbf{x}_i - \mathbf{x}_c) + \boldsymbol{\Lambda}[\mathbf{f}\,](s_i) + \mathbf{K}_\delta[\mathbf{f}\,](s_i) = \mathbf{U}_0(\mathbf{x}_i)\,, i = 0,\ldots,M \\ \sum_{i=0}^{M} \alpha_i\, \mathbf{f}_i \ = 0 \ \ , \qquad \sum_{i=0}^{M} \alpha_i\, (\mathbf{x}_i - \mathbf{x}_c) \times \mathbf{f}_i \ = 0 \end{gathered} \tag{0.25}$$

where $\alpha_i = \begin{cases} \Delta s/2 & , i = 0, M \\ \Delta s & , \ o.w \end{cases}$.

The unknowns are the vectors $\mathbf{f}_i, i = 0,..,M$, together with $\mathbf{V}$ and $\boldsymbol{\Omega}$, a total of $3(M+1)+6$ unknowns. The number of equations is the same, with $3(M+1)$ equations on the first line of (0.25) and the remaining 6 on the second line. Note that the centroid $\mathbf{x}_c = (x_c, y_c, z_c)$ is computed as [20].

$$x_c = \frac{1}{M+1}\sum_{i=0}^{M} x_i \quad , \quad y_c = \frac{1}{M+1}\sum_{i=0}^{M} y_i \quad , \quad z_c = \frac{1}{M+1}\sum_{i=0}^{M} z_i \tag{0.26}$$

3.3 Evaluation of $\mathbf{K_\delta[f\,]}$

Rewrite $\mathbf{K}_\delta[\mathbf{f}\,](s)$ as two separate integrals, I_1 and I_2

$$\mathbf{K}_\delta[\mathbf{f}\,](s) = \underbrace{\int_0^1 \frac{\mathbf{I}+\widehat{\mathbf{R}}(s,s')\widehat{\mathbf{R}}(s,s')}{\sqrt{|\mathbf{R}(s,s')|^2+\delta^2}}\mathbf{f}(s')ds'}_{I_1(s)} + \underbrace{\int_0^1 -\frac{\mathbf{I}+\mathbf{T}(s)\mathbf{T}(s)}{\sqrt{|s-s'|^2+\delta^2}}\,\mathbf{f}(s)ds'}_{I_2(s)} \tag{0.27}$$

The first integral I_1 can be approximated using trapezoidal method, i.e,

$$I_1(s) \cong \sum_{j=0}^{M} \underbrace{\alpha_j \frac{\mathbf{I}+\widehat{\mathbf{R}}(s,s_j)\widehat{\mathbf{R}}(s,s_j)}{\sqrt{|\mathbf{R}(s,s_j)|^2+\delta^2}}}_{K_1(s,s_j)}\,\mathbf{f}_j = \sum_{j=0}^{M} K_1(s,s_j)\;\mathbf{f}_j \tag{0.28}$$

The second integral I_2 can be evaluated analytically. As the integral

$$\int_0^1 -\frac{1}{\sqrt{|s-s'|^2+\delta^2}}\,ds' = log\left(\frac{\sqrt{(s-1)^2+\delta^2}+s-1}{\sqrt{s^2+\delta^2}+s}\right)$$

then I_2 can have the following closed formula

$$I_2(s) = \underbrace{log\left(\frac{\sqrt{(s-1)^2+\delta^2}+s-1}{\sqrt{s^2+\delta^2}+s}\right)[\mathbf{I}+\mathbf{T}(s)\mathbf{T}(s)]}_{K_2(s)}\,\mathbf{f}(s) = K_2(s)\mathbf{f}(s) \tag{0.29}$$

K_1 and K_2 are 3×3 matrices. Then

$$\mathbf{K}_\delta[\mathbf{f}\,](s) = \sum_{j=0}^{M} K_1(s,s_j)\;\mathbf{f}_j + K_2(s)\mathbf{f}(s) \tag{0.30}$$

Now we write an approximation of $\mathbf{K_\delta[f\,]}$ as

$$\mathbf{K}_\delta[\mathbf{f}\,](s_i) = \sum_{j=0}^{M} K_1(s_i,s_j)\;\mathbf{f}_j + K_2(s_i)\mathbf{f}_i \;,\quad i = 0,1,\dots,M \tag{0.31}$$

Eq. (0.31) can be written in matrix form as

$$\mathbf{K}_\delta[\mathbf{f}\,] = \underbrace{\begin{bmatrix} K_1(s_0,s_0)+K_2(s_0) & K_1(s_0,s_1) & \cdots & K_1(s_0,s_M) \\ K_1(s_1,s_0) & K_1(s_1,s_1)+K_2(s_1) & & \vdots \\ \vdots & & \ddots & K_1(s_{M-1},s_M) \\ K_1(s_M,s_0) & \cdots & K_1(s_M,s_{M-1}) & K_1(s_M,s_M)+K_2(s_M) \end{bmatrix}}_{\mathcal{K}} \underbrace{\begin{bmatrix} \mathbf{f}_0 \\ \mathbf{f}_1 \\ \vdots \\ \mathbf{f}_{M-1} \\ \mathbf{f}_M \end{bmatrix}}_{\mathcal{F}}$$

$$\mathbf{K}_\delta[\mathbf{f}\,] = \boldsymbol{\mathcal{K}}\boldsymbol{\mathcal{F}} \tag{0.32}$$

where $\boldsymbol{\mathcal{K}}$ is $3(M+1)\times 3(M+1)$ matrix and $\boldsymbol{\mathcal{F}}$ is $3(M+1)$ column vector. Note that $\mathbf{f}_i = (f_{ix} \quad f_{iy} \quad f_{iz})^T$.

3.4 The Rest of the Equation

Similarly we discretize the rest of the equation:

$$\boldsymbol{\Lambda}[\mathbf{f}\,](s_i) = \underbrace{[-c(\mathbf{I}+\mathbf{T}_i\,\mathbf{T}_i)+2(\mathbf{I}-\mathbf{T}_i\,\mathbf{T}_i)]}_{D(s_i)}\mathbf{f}_i = D(s_i)\mathbf{f}_i \tag{0.33}$$

where D is a 3×3 matrix. In matrix form, Eq. (0.33) can be written as

$$\boldsymbol{\Lambda}[\mathbf{f}\,](s_i) = \underbrace{\begin{bmatrix} D(s_0) & \mathbf{0} & \cdots & \mathbf{0} \\ \mathbf{0} & D(s_1) & & \vdots \\ \vdots & & \ddots & \mathbf{0} \\ \mathbf{0} & \cdots & \mathbf{0} & D(s_M) \end{bmatrix}}_{\boldsymbol{\mathcal{D}}} \underbrace{\begin{bmatrix} \mathbf{f}_0 \\ \mathbf{f}_1 \\ \vdots \\ \mathbf{f}_{M-1} \\ \mathbf{f}_M \end{bmatrix}}_{\boldsymbol{\mathcal{F}}} = \boldsymbol{\mathcal{D}}\boldsymbol{\mathcal{F}} \tag{0.34}$$

where $\boldsymbol{\mathcal{D}}$ is $3(M+1)\times 3(M+1)$ matrix, and $\mathbf{0}$ is a 3×3 zero matrix. The velocity term $(\mathbf{V}+\boldsymbol{\Omega}\times(\mathbf{x}_i-\mathbf{x}_c))$ can be written in matrix form as

$$\underbrace{\begin{bmatrix} I & O_0 \\ I & O_1 \\ \vdots & \vdots \\ I & O_M \end{bmatrix}}_{3(M+1)\times 6} \begin{bmatrix} \mathbf{V} \\ \boldsymbol{\Omega} \end{bmatrix} \tag{0.35}$$

where I is the 3×3 identity matrix, and

$$O_i = \begin{bmatrix} 0 & (\mathbf{x}_i-\mathbf{x}_c)_z & -(\mathbf{x}_i-\mathbf{x}_c)_y \\ -(\mathbf{x}_i-\mathbf{x}_c)_z & 0 & (\mathbf{x}_i-\mathbf{x}_c)_x \\ (\mathbf{x}_i-\mathbf{x}_c)_y & -(\mathbf{x}_i-\mathbf{x}_c)_x & 0 \end{bmatrix}, \text{ and } \begin{bmatrix} \mathbf{V} \\ \boldsymbol{\Omega} \end{bmatrix} = [V_x \;\; V_y \;\; V_z \;\; \omega_x \;\; \omega_y \;\; \omega_z]^T.$$

The right-hand side can written as

$$\mathbf{U}_0 = [\mathbf{U}_0(\mathbf{x}_0) \quad \mathbf{U}_0(\mathbf{x}_1) \quad \cdots \quad \mathbf{U}_0(\mathbf{x}_{M-1}) \quad \mathbf{U}_0(\mathbf{x}_M)]^T \tag{0.36}$$

where $\mathbf{U}_0(\mathbf{x}_i) = [U_0(\mathbf{x}_i)_x \quad U_0(\mathbf{x}_i)_y \quad U_0(\mathbf{x}_i)_z]^T$.

3.5 Constraints

We used trapezoidal method to approximate the integral over the force and torque. These approximations can be written in matrix form as

$$\sum_{i=0}^{M} \alpha_i \, \mathbf{f}_i = \underbrace{[\alpha_0 I \quad \alpha_1 I \quad \cdots \quad \alpha_M I]}_{3\times 3(M+1)} \begin{bmatrix} \mathbf{f}_0 \\ \vdots \\ \mathbf{f}_M \end{bmatrix} = 0 \tag{0.37}$$

and

$$\sum_{i=0}^{M} \alpha_i \, (\mathbf{x}_i - \mathbf{x}_c) \times \mathbf{f}_i = \underbrace{[\alpha_0 C_0 \quad \alpha_1 C_1 \quad \cdots \quad \alpha_M C_M]}_{3\times 3(M+1)} \begin{bmatrix} \mathbf{f}_0 \\ \vdots \\ \mathbf{f}_M \end{bmatrix} = 0 \tag{0.38}$$

where

$$C_i = \begin{bmatrix} 0 & -(\mathbf{x}_i - \mathbf{x}_c)_z & (\mathbf{x}_i - \mathbf{x}_c)_y \\ (\mathbf{x}_i - \mathbf{x}_c)_z & 0 & -(\mathbf{x}_i - \mathbf{x}_c)_x \\ -(\mathbf{x}_i - \mathbf{x}_c)_y & (\mathbf{x}_i - \mathbf{x}_c)_x & 0 \end{bmatrix}$$

3.6 Full System

Using Eqs. (0.32) - (0.38) the full system can be presented in matrix form as

$$\overbrace{\underbrace{\left[\begin{array}{cc|ccc} I & O_0 & & & \\ I & O_1 & & & \\ \vdots & \vdots & & \mathcal{K}+\mathcal{D} & \\ & & & & \\ I & O_M & & & \\ \hline \mathbf{0} & \mathbf{0} & \alpha_0 I & \cdots & \alpha_M I \\ \mathbf{0} & \mathbf{0} & \alpha_0 C_0 & \cdots & \alpha_M C_M \end{array}\right]}_{3(M+3)\times 3(M+3)}}^{\mathcal{A}} \overbrace{\underbrace{\begin{bmatrix} \mathbf{V} \\ \boldsymbol{\Omega} \\ \mathbf{f}_0 \\ \mathbf{f}_1 \\ \vdots \\ \mathbf{f}_{M-1} \\ \mathbf{f}_M \end{bmatrix}}_{3(M+3)\times 1}}^{\mathcal{X}} = \overbrace{\underbrace{\begin{bmatrix} \mathbf{U}_0(\mathbf{x}_0) \\ \mathbf{U}_0(\mathbf{x}_1) \\ \\ \vdots \\ \\ \mathbf{U}_0(\mathbf{x}_M) \\ 0 \\ 0 \end{bmatrix}}_{3(M+3)\times 1}}^{\mathcal{b}} \Rightarrow \mathcal{A}\mathcal{X} = \mathcal{b} \tag{0.39}$$

where $\mathcal{K}$ and $\mathcal{D}$ are defined in equations (0.32) and (0.34) respectively. Now we can solve for $\boldsymbol{\mathcal{X}}$ to find the velocities $\boldsymbol{V}$ and $\boldsymbol{\Omega}$, and the forces $\mathbf{f_0}, \ldots, \mathbf{f_M}$.

4 Multiple Fibers

In addition to what we have done in sec 3, we discretize the integral term $\int_0^1 \mathbf{G}(\mathbf{R}^l)\mathbf{f}^l(s')ds'$ in Eq.(0.20). First we rewrite Eq. (0.20)as

$$\mathbf{V}^n + \boldsymbol{\Omega}^n \times (\mathbf{x}^n(s) - \mathbf{x}_c^n) + \boldsymbol{\Lambda}^n[\mathbf{f}^n\,](s) + \mathbf{K}^n{}_\delta[\mathbf{f}^n\,](s) - \sum_{\substack{l=1 \\ l\neq n}}^{N} \int_0^1 \mathbf{G}(\mathbf{R}^l(s,s'))\mathbf{f}^l(s')ds' = \mathbf{U}_0\big(\mathbf{x}^n(s)\big) \tag{0.40}$$

For simplicity, let us write $\mathbf{G}(s,s') = \mathbf{G}(\mathbf{R}^l(s,s'))$. We use the same method that we have used in sec 2.2. The centerline of fiber l is discretized by the parameter $s_j' = j\Delta s', i = 0,1,\dots,M$, where $\Delta s' = 1/M$. Then the integral term can be approximated as

$$\int_0^1 \mathbf{G}(s,s')\,\mathbf{f}^l(s')ds' \;\cong\; \sum_{j=0}^{M} \alpha_j\,\mathbf{G}\big(s,s_j'\big)\,\mathbf{f}_j^l \tag{0.41}$$

where $\alpha_j = \begin{cases} \Delta s'/2 & ,j = 0, M \\ \Delta s' & ,\ o.w \end{cases}$.

Then we discretize the centerline of the fiber n by the parameter $s_i = i\Delta s, i = 0,1,\dots,M$, where $\Delta s = \frac{1}{M}$. The equation and the constraints become

$$\mathbf{V}^n + \boldsymbol{\Omega}^n \times (\mathbf{x}_i^n - \mathbf{x}_c^n) + \boldsymbol{\Lambda}^n[\mathbf{f}_i^n\,] + \mathbf{K}^n{}_\delta[\mathbf{f}_i^n\,] - \sum_{\substack{l=1 \\ l\neq n}}^{N}\sum_{j=0}^{M} \alpha_j\,\mathbf{G}\big(s_i,s_j'\big)\,\mathbf{f}_j^l = \mathbf{U}_0(\mathbf{x}_i^n) \tag{0.42}$$

$$\sum_{i=0}^{M} \alpha_i\,\mathbf{f}_i^n = 0 \quad , \qquad \sum_{i=0}^{M} \alpha_i\,(\mathbf{x}_i^n - \mathbf{x}_c^n) \times \mathbf{f}_i^n = 0$$

According to Eq. (0.39) the quantity $(\mathbf{V}^n + \boldsymbol{\Omega}^n \times (\mathbf{x}_i^n - \mathbf{x}_c^n) + \boldsymbol{\Lambda}^n[\mathbf{f}_i^n\,] + \mathbf{K}^n{}_\delta[\mathbf{f}_i^n\,])$ can be written in matrix form as

$$\boldsymbol{\mathcal{A}^n}\boldsymbol{\mathcal{X}^n} = \boldsymbol{\mathcal{b}^n} \tag{0.43}$$

where

$$\boldsymbol{\mathcal{A}^n} = \left[\begin{array}{ccc|ccc} I & O_0^n & | & & & \\ I & O_1^n & | & & \mathcal{K}^n + \mathcal{D}^n & \\ \vdots & \vdots & | & & & \\ & & | & & & \\ I & O_M^n & | & & & \\ \hline \mathbf{0} & \mathbf{0} & | & \alpha_0 I & \cdots & \alpha_M I \\ \mathbf{0} & \mathbf{0} & | & \alpha_0 C_0^n & \cdots & \alpha_M C_M^n \end{array}\right], \boldsymbol{\mathcal{X}^n} = \begin{bmatrix} \mathbf{V}^n \\ \boldsymbol{\Omega}^n \\ \mathbf{f}_0^n \\ \mathbf{f}_1^n \\ \vdots \\ \mathbf{f}_{M-1}^n \\ \mathbf{f}_M^n \end{bmatrix}, \boldsymbol{\mathcal{b}^n} = \begin{bmatrix} \mathbf{U}_0(\mathbf{x}_0^n) \\ \mathbf{U}_0(\mathbf{x}_1^n) \\ \\ \vdots \\ \\ \mathbf{U}_0(\mathbf{x}_M^n) \\ 0 \\ 0 \end{bmatrix}$$

where $\mathcal{K}^n$, $\mathcal{D}^n$, O_i^n and C_i^n were defined in Eqs. (0.32), (0.34), (0.35) and (0.38), respectively, as $\mathcal{K}$, $\mathcal{D}$, O_i and C_i.

The remaining summation term can be written in matrix form as

$$\sum_{j=0}^{M} \alpha_j \, \mathbf{G}(s_i, s_j') \, \mathbf{f}_j^l = \begin{bmatrix} \alpha_0\mathbf{G}(s_0,s_0') & \alpha_1\mathbf{G}(s_0,s_1') & \cdots & \alpha_M\mathbf{G}(s_0,s_M') \\ \alpha_0\mathbf{G}(s_1,s_0') & \alpha_1\mathbf{G}(s_1,s_1') & \dots & \vdots \\ \vdots & & \ddots & \\ \alpha_0\mathbf{G}(s_M,s_0') & \cdots & & \alpha_M\mathbf{G}(s_M,s_M') \end{bmatrix} \begin{bmatrix} \mathbf{f}_0^l \\ \mathbf{f}_1^l \\ \vdots \\ \mathbf{f}_{M-1}^l \\ \mathbf{f}_M^l \end{bmatrix} = H_{nl}\boldsymbol{\mathcal{F}}^l \,, l \neq n \tag{0.44}$$

where $s_i \epsilon \Gamma_n$ and $s'_j \epsilon \Gamma_l$, $i, j = 0, \dots, M$.

Let $\boldsymbol{\mathcal{H}_{nl}}$ be

$$\boldsymbol{\mathcal{H}_{nl}} = \underbrace{\left[\begin{array}{cc|ccc|c} \mathbf{0} & \mathbf{0} & & & & \\ \mathbf{0} & \mathbf{0} & & & & \\ \vdots & \vdots & & & H_{nl} & \\ & & & & & \\ \mathbf{0} & \mathbf{0} & & & & \\ \hline \mathbf{0} & \mathbf{0} & \mathbf{0} & \mathbf{0} & \mathbf{0} & \mathbf{0} \\ \mathbf{0} & \mathbf{0} & \mathbf{0} & \mathbf{0} & \mathbf{0} & \mathbf{0} \end{array}\right]}_{(3(M+1)+6)\times(3(M+1)+6)} \tag{0.45}$$

Then the full system for N fibers can be written as

$$\underbrace{\begin{bmatrix} \boldsymbol{\mathcal{A}^1} & \boldsymbol{\mathcal{H}_{12}} & \boldsymbol{\mathcal{H}_{13}} & \dots & & \boldsymbol{\mathcal{H}_{1N}} \\ \boldsymbol{\mathcal{H}_{21}} & \boldsymbol{\mathcal{A}^2} & \boldsymbol{\mathcal{H}_{23}} & \dots & & \boldsymbol{\mathcal{H}_{2N}} \\ \boldsymbol{\mathcal{H}_{31}} & \boldsymbol{\mathcal{H}_{32}} & \boldsymbol{\mathcal{A}^3} & \boldsymbol{\mathcal{H}_{34}} & \dots & \boldsymbol{\mathcal{H}_{3N}} \\ \vdots & \vdots & & \ddots & \vdots & \\ & & & \boldsymbol{\mathcal{A}^{N-1}} & \boldsymbol{\mathcal{H}_{(N-1)N}} & \\ \boldsymbol{\mathcal{H}_{N1}} & \boldsymbol{\mathcal{H}_{N2}} & \cdots & \boldsymbol{\mathcal{H}_{N(N-1)}} & \boldsymbol{\mathcal{A}^N} & \end{bmatrix}}_{3N(M+3)\times 3N(M+3)} \underbrace{\begin{bmatrix} \boldsymbol{\mathcal{X}^1} \\ \boldsymbol{\mathcal{X}^2} \\ \\ \vdots \\ \boldsymbol{\mathcal{X}^{N-1}} \\ \boldsymbol{\mathcal{X}^N} \end{bmatrix}}_{3N(M+3)\times 1} = \underbrace{\begin{bmatrix} \boldsymbol{\mathcal{b}^1} \\ \boldsymbol{\mathcal{b}^2} \\ \\ \vdots \\ \boldsymbol{\mathcal{b}^{N-1}} \\ \boldsymbol{\mathcal{b}^N} \end{bmatrix}}_{3N(M+3)\times 1} \tag{0.46}$$

$$\boldsymbol{\mathcal{A}^* \mathcal{X}^* = \mathcal{b}^*}$$

Now we can solve for $\boldsymbol{\mathcal{X}^*}$ to find the velocities $\mathbf{V}^n$ and $\boldsymbol{\Omega}^n$, and the forces $\mathbf{f_0^n}, \dots, \mathbf{f_M^n}$ for each fiber Γ^n.

5 Convergence and Accuracy

Since the exact solution of the problem is not known, to test the convergence of our numerical method a number of test runs are performed for different time-step, Δt, and spatial-step Δs. Unless mentioned otherwise, all runs are performed with constant shear rate $\dot{\gamma} = 1$, and constant curvature ($\kappa = 20$) and torsion ($\tau = 4$).

The order of convergence is determined by measuring the difference in fiber positions at the end time ($t = 1$) of consecutive solutions that are computed by changing one of the parameters while the other is kept fixed. The fiber position and orientation vectors are updated using the second order methods in Eq. (0.22) and Eq. (0.23), respectively.

To check the convergence in time, six sets of runs have been made with $\Delta t = \frac{1}{32}, \frac{1}{64}, \frac{1}{128}, \frac{1}{256}, \frac{1}{512}$ and $\frac{1}{1024}$. For the fiber with position $(\mathbf{x}, \mathbf{y}, \mathbf{z})$, obtained with Δt and for the same fiber but with position $(\hat{\mathbf{x}}, \hat{\mathbf{y}}, \hat{\mathbf{z}})$ obtained with $\frac{\Delta t}{2}$, we define the difference as

$$e = \left(\frac{1}{M} \sum_{i=0}^{M} (x_i - \hat{x}_i)^2 + (y_i - \hat{y}_i)^2 + (z_i - \hat{z}_i)^2 \right)^{\frac{1}{2}} \tag{0.47}$$

where $\mathbf{x}$, $\mathbf{y}$, $\mathbf{z}$, and $\hat{\mathbf{x}}$, $\hat{\mathbf{y}}$, $\hat{\mathbf{z}}$ are $(M+1)$ column vectors. The results are presented in Fig. 1. We used $\Delta s = \frac{1}{64}$ $(M = 63)$.

Based on the consecutive solutions, the rate of convergence varies between 1.995 and 2.009 which is very close to the second order accuracy expected for our numerical method. Moreover, in this case we got an error of order 10^{-4} when $\Delta t = \frac{1}{32} \approx 0.0313$ which is sufficiently accurate for our purposes.

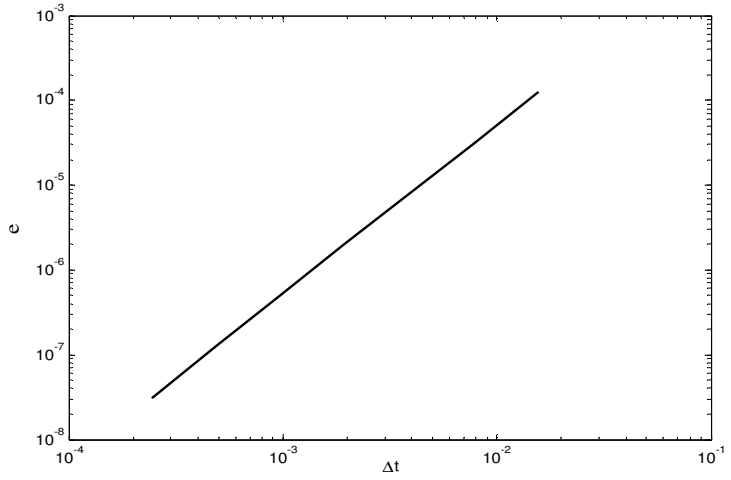

Fig. 1. *loglog* plot of the error in fiber position plotted as a function of Δt at the end time $t = 1$. In this case $\Delta s = \frac{1}{64}$

As for spatial convergence, we performed five runs with $\Delta s = \frac{1}{16}, \frac{1}{32}, \frac{1}{64}, \frac{1}{128}, \frac{1}{256}$. In the same manner, for the fiber $(\mathbf{x}, \mathbf{y}, \mathbf{z})$ obtained at $t = 1$ with Δs and for the fiber $(\hat{\mathbf{x}}, \hat{\mathbf{y}}, \hat{\mathbf{z}})$ obtained at $t = 1$ with $\frac{\Delta s}{2}$, we define the difference as before. The results are given in Fig. 2. Here we used $\Delta t = \frac{1}{32}$. The rate of convergence varies between 1.866 and 2.340. In this case the error is of order 10^{-3} when $\Delta s = \frac{1}{32} = 0.0313$.

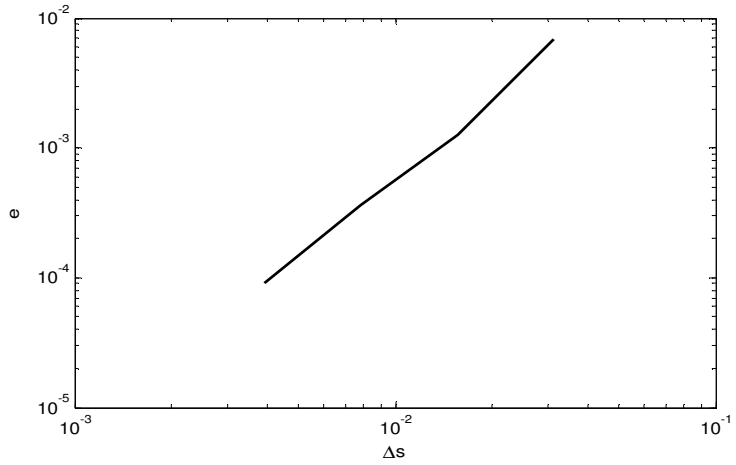

Fig. 2. *loglog* plot of the error in fiber position plotted as a function of Δs at the end time $t = 1$. In this case $\Delta t = \frac{1}{32}$

Note that the same approach has been followed to determine the rate of convergence in the case of single fiber sedimenting due to gravity. Almost the same rates of convergence have been gotten. Time refinements gave a rate varying between 1.98 and 2.01, whereas spatial refinements gave a rate between 1.78 and 2.16, which are, as expected, very close to second order accuracy.

6 Numerical Results

6.1 Shear flow

In this section, we present numerical simulations of a single fiber suspension in shear flow, and discuss some results.

Fig. 3 presents the configuration of the fiber at three different times of a simulation with single fiber in shear flow with constant shear rate $\dot{\gamma} = 1$ ($U_0 = y$) .

In Fig. 3, the initial orientation has been determined according to the initial frame $\mathbf{Q}_0 = (\mathbf{T}_0\ \mathbf{N}_0\ \mathbf{B}_0)$ where $\mathbf{T}_0 = \frac{1}{\sqrt{1+0.2^2}}(1\ 0\ .2) = (0.9806\ \ 0\ \ 0.1961)$, $\mathbf{N}_0 = (0\ 1\ 0)$ and $\mathbf{B}_0 = \mathbf{T} \times \mathbf{N}$. As in previous section, we used constant curvature ($\kappa = 20$) and torsion ($\tau = 4$). The aspect ratio used in the simulation is $\varepsilon = 0.0001$, $\Delta s = \frac{1}{64}$ and $\Delta t = \frac{1}{32}$.

Jeffery [1] studied a single ellipsoidal fiber rotating in a Newtonian, incompressible, homogeneous flow. In Jeffery's theory, the fiber orientation is defined by three angles (φ, θ, ψ) in terms of the global coordinate system xyz, where a local coordinate system $x'\ y'z'$ translates and rotates with the fiber [1,10,21], see Fig 4. Jeffery assumed that the ellipsoidal fiber's center translates with the same linear velocity as the undisturbed simple shear flow evaluated at the fiber

centroid. Formulas of (φ, θ, ψ) have been found by Jeffery. Jeffery's formulas predict a periodical behavior for a fiber in a pure shearing flow with an orbital period [22].

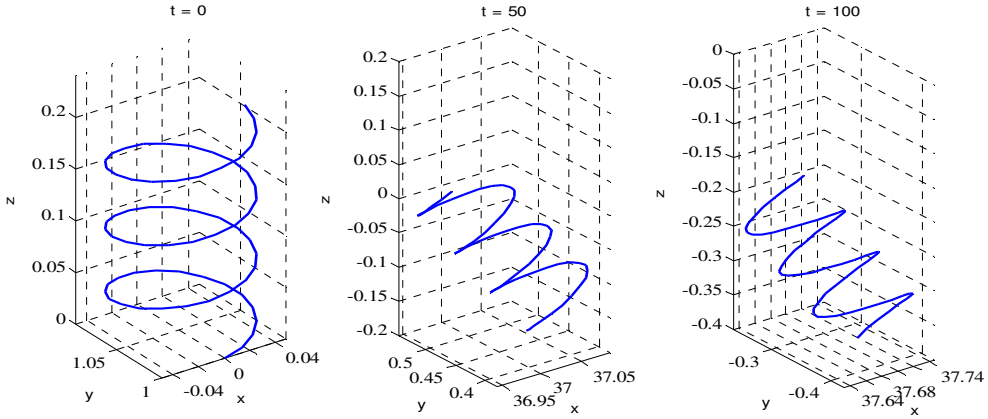

Fig. 3. Fiber configuration with $\kappa = 20$ and $\tau = 4$ at $t = 0, t = 50$ and $t = 100$ in shear flow

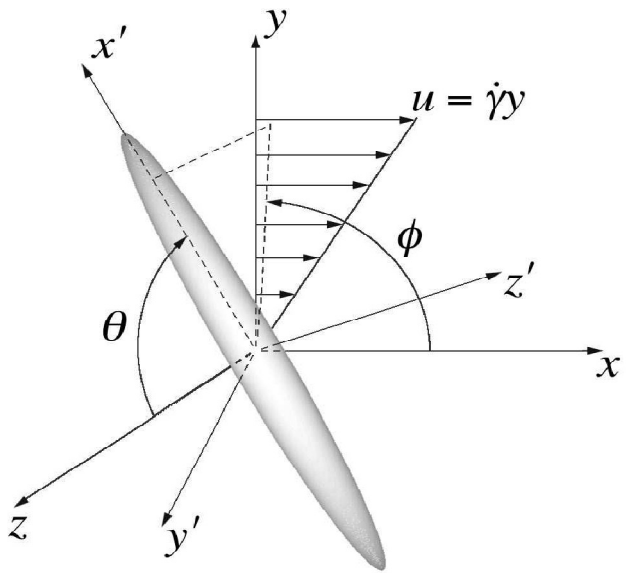

Fig. 4. Coordinate system for ellipsoidal fiber suspended in a shear flow

Unfortunately, we don't have such formulas for the same angles in the curved fiber case; therefore, we defined the angle θ as the angle between the helix axis and the xy-plane. This angle will give an indication about the fiber orientation.

The helix axis needs to be determined first. Many approaches have been suggested to define the helix axis [20,23,24]. Here we will use the method suggested in [20]. Approximate local centroids, $\mathbf{x}_c^i = (x_c^i, y_c^i, z_c^i)$, of the helix were determined by dividing the helix into parts and computing the centroid of each part. The helix axis will be the line that passes through these. Once we have the helix axis, we compute the angle θ.

In Fig. 5, the angle θ is shown as a function of time t. Looking at Fig. 5 we see that there is a drift between $t = 0$ and $t = 100$, the drift mainly occurs due to the initial orientation of the fiber. This can be explained by observing the dynamical process. After some time, $t = 100$, θ starts having a periodic behavior with a period of length $T = 10.4$ and lies in the interval (0.38, 0.62).

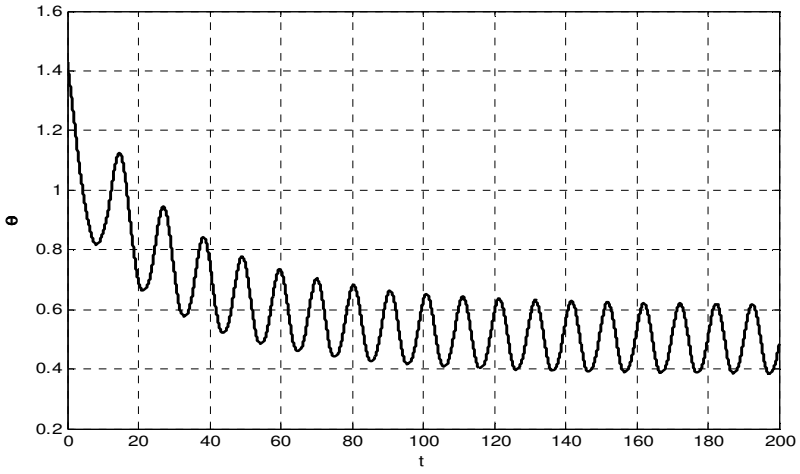

Fig. 5. Angle θ as a function of time t for a helix

To make a comparison, we perform a run of a straight fiber, i.e. $\kappa = 0$ and $\tau = 0$. All other numerical parameters are kept as we defined them for the curved fiber case, i.e. $\mathbf{T}_0 = (0.9806\ \ 0\ \ 0.1961)$, $\mathbf{N}_0 = (0\ 1\ 0)$ and $\mathbf{B}_0 = \mathbf{T} \times \mathbf{N}$, $\varepsilon = 0.0001$, $\Delta s = \frac{1}{64}$ and $\Delta t = 1/32$.

In this case we measure the angle $\theta_{straight}$ between the fiber's centerline and xy-plane. In Fig. 6, $\theta_{straight}$ is shown as a function of time. As expected, we have a periodical behavior and we compute the period $T = 3.625$.

Back to curved fiber, with the same numerical parameter but the initial frame, we performed three runs using three different initial configurations according to $\mathbf{T}_0 = (1/\sqrt{1 + T_z^2})\,(1\ 0\ T_z)$, where $T_z = 1, 0.2$ and 0.

In Fig. 7 the trajectory of the centroid in xy-plane is shown. We observe that we have periodic trajectories with different periods according to the initial orientation. Moreover, we can see that the initial orientation strongly affects the drift of these trajectories.

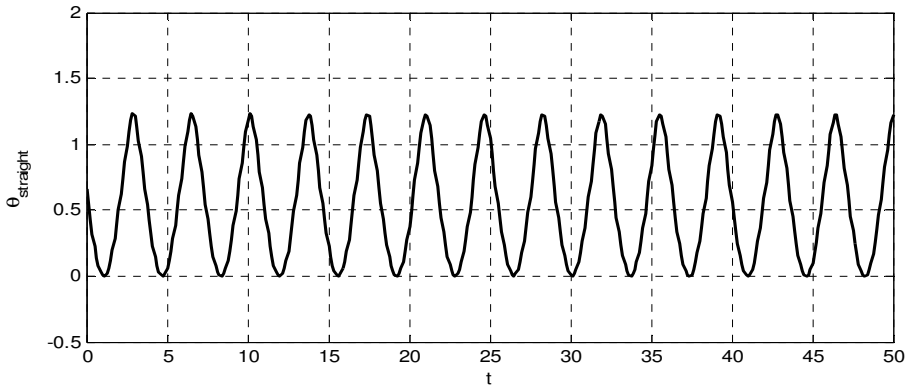

Fig. 6. Angle $\theta_{straight}$ as a function of time t for a straight fiber

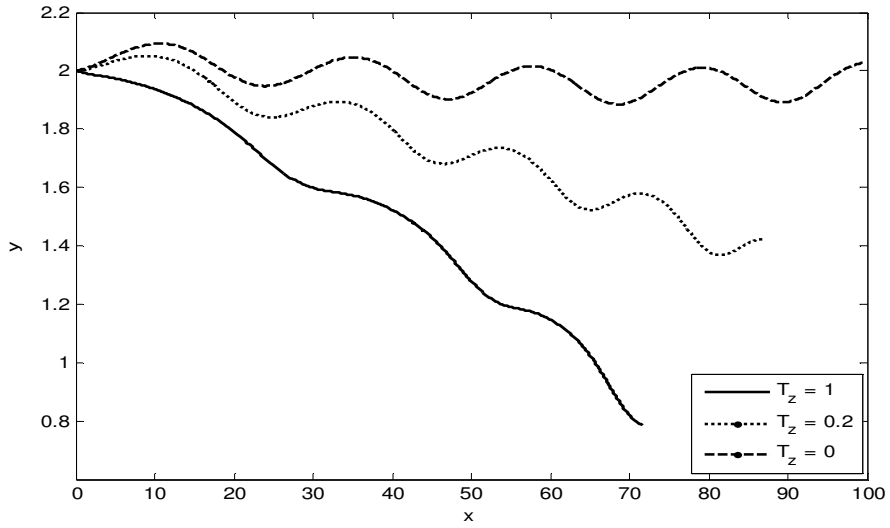

Fig. 7. Trajectories of the fiber's centroid with different initial configuration in shear flow

6.2 Sedimentation

In this section the case of one single fiber sedimenting due to gravity is considered. The gravity is acting in the negative z-direction. First, we investigate the fiber's sedimentation speed by performing a run using the same previous numerical parameters. Fig. 8 presents the sedimentation speed as a function of time t. Looking at Fig. 8, we observe that the speed fluctuating between 1.21 and 1.42. The reason behind this fluctuation in the speed is that orientation of the fiber is changing with time.

For example, between $t = 11$ and $t = 15$, the sedimentation speed increases from a local bottom 1.2149 to a local peak 1.3753. The orientation of the helix axis within this time interval varies from $\theta = 1.11$ rad at $t = 11$ to being almost parallel to xy-plane with $\theta = 0.0039$ rad at $t = 15$, see Fig. 9(a), and the speed starts decreasing after $t = 15$.

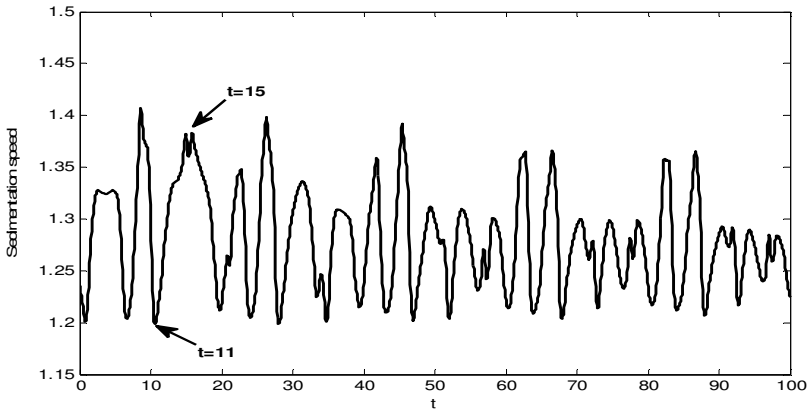

Fig. 8. Sedimentation speed of one fiber

In Fig. 9, the angle between helix axis and xy-plane within the time interval $[11,15]$ is shown (a) as a function on time, and (b) as a function of sedimentation speed. According to Fig. 8 and Fig. 9 we conclude that the sedimentation speed decreases as θ increases.

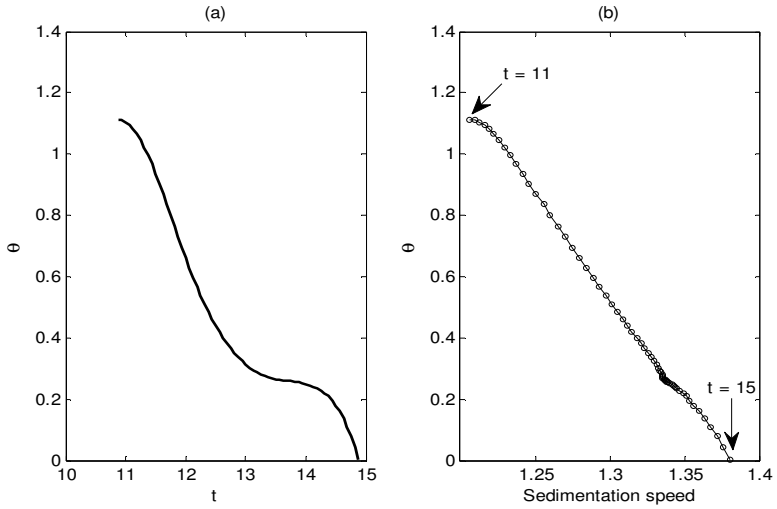

Fig. 9. Angle θ between the helix axis and xy-plan within the time interval [11,15] (a) as a function of time (b) as a function of sedimentation speed

Using the same run we plot the trajectory of the fiber's centriod in xz-plane, see Fig 10, where we note a drift and irregular displacement in the x-direction.

Next we performed three runs where $T_z = 0$ and the other numerical parameters were kept as previously determined. However, we used different curvatures and torsions. We considered the following combinations: $(\kappa = 1, \tau = 1)$, $(\kappa = 10, \tau = 10)$ and $(\kappa = 30, \tau = 10)$.

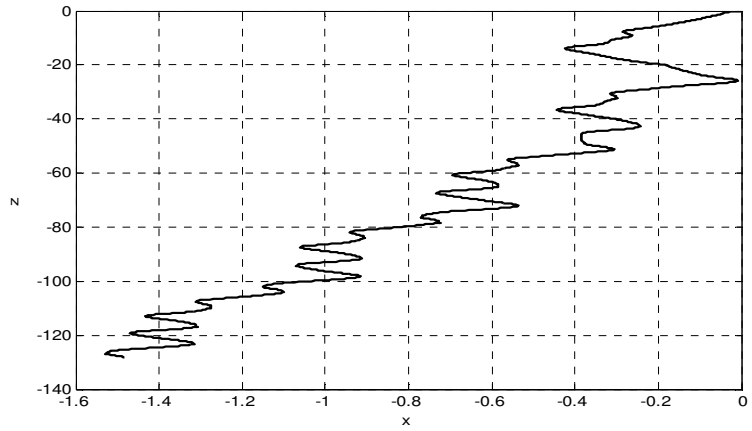

Fig. 10. Trajectory of the fiber's centroid in xz-plane

In Fig. 11, we present the trajectories of fiber's centroids. They look very different from each other. No conclusion can be addressed regarding the relation between the curvature and torsion, and the behavior of the fiber. However, the figure can give indication about the relation between curvature and sedimentation speed.

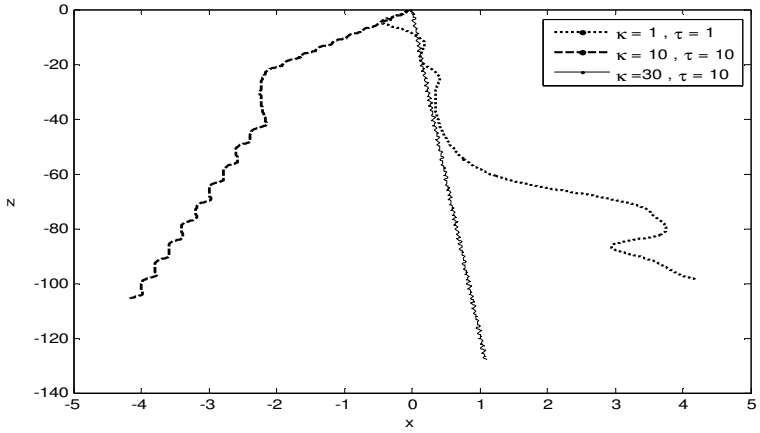

Fig. 11. Trajectories of fiber's centroids with different curvatures and torsions

Next we performed 15 runs with the same three combinations as above and for five different initial orientations according to $\mathbf{T}_0 = (1/\sqrt{1+T_z^2})\,(1\ 0\ T_z)$ where $T_z = 1.3, 0.7, 0.2, 0$ and -0.7. Again, we observe that the initial orientation has a great influence on the fiber's behavior. But here we can see also the larger curvature we use the more regular trajectories we get.

To have a better indication about the influence of the curvature on the sedimentation speed, we perform four runs with fixed torsion $\tau = 10$ and four different values of curvature, $\kappa = 20, 30, 40$ and 50, $t\epsilon[0,50]$. The average sedimentation speed as a function of the curvature is shown in Fig. 12. The thing that can be seen is that the larger the curvature we use the higher the sedimentation speed we get.

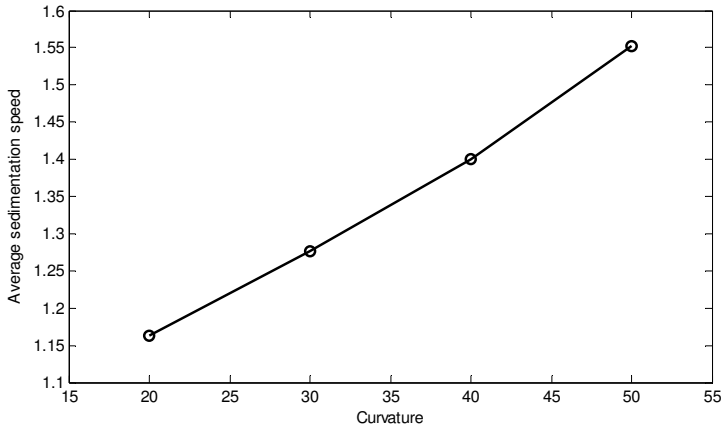

Fig. 12. Average sedimentation speed as a function of curvature

Centroids trajectories in xz-plane and yz-plane are shown in Fig. 13. The figure agrees with the conclusion that we have made before, moreover, we observe that the fiber with higher curvature is sedimenting more perpendicularly than that with lower curvature.

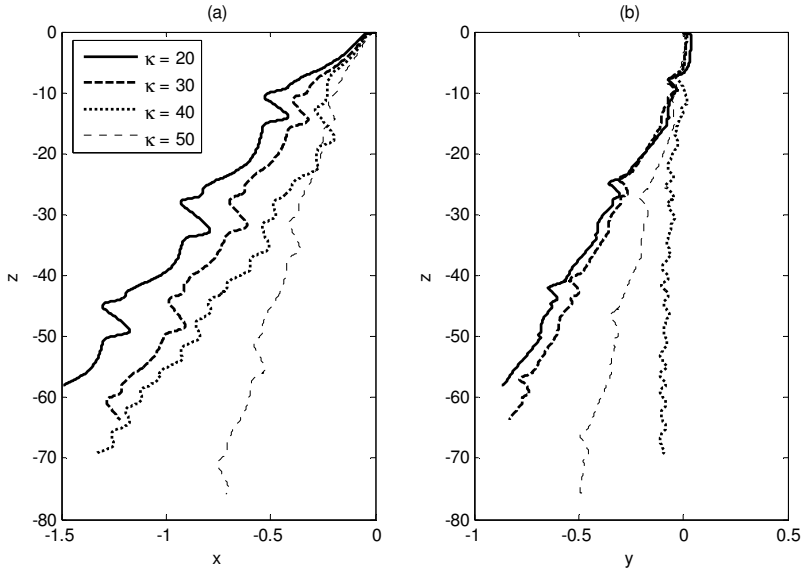

Fig 13. Trajectories of the fibers centroids with $\kappa = 20, 30, 40$ and 50 (a) in xz-plane, and (b) in yz-plane

6.3 Multiple Fibers

In this section we consider the case of multiple fibers sedimenting due to gravity. We present numerical simulations of collections of 2, 3 and 4 fibers and discuss a variety of results obtained. Here we are interested in identical fibers. To construct identical fibers we use the same initial orientation frame, $\mathbf{Q}_0 = (\mathbf{T}_0\ \mathbf{N}_0\ \mathbf{B}_0)$ and the same curvature and torsion, and we choose different initial points, x_0^j, where $j = 1,2,\dots,N$ are the indices of fibers. Initially, we determined the initial points as vertices of "*N*-sided" regular polygon.

First, we perform a simulation of 2, 3 and 4 fibers using the initial frame $\mathbf{T}_0 = \frac{1}{\sqrt{1+0.2^2}}(1\ 0\ .2)$, $\mathbf{N}_0 = (0\ 1\ 0)$ and $\mathbf{B}_0 = \mathbf{T} \times \mathbf{N}$, $\kappa = 20$ and $\tau = 4$. The average sedimentation speed is obtained, see Fig. 14. Looking at Fig. 14 we observe that at the beginning the sedimentation speed is slightly higher when $N = 4$, however, at the end of the simulation, the sedimentation speed for different cases became much closer.

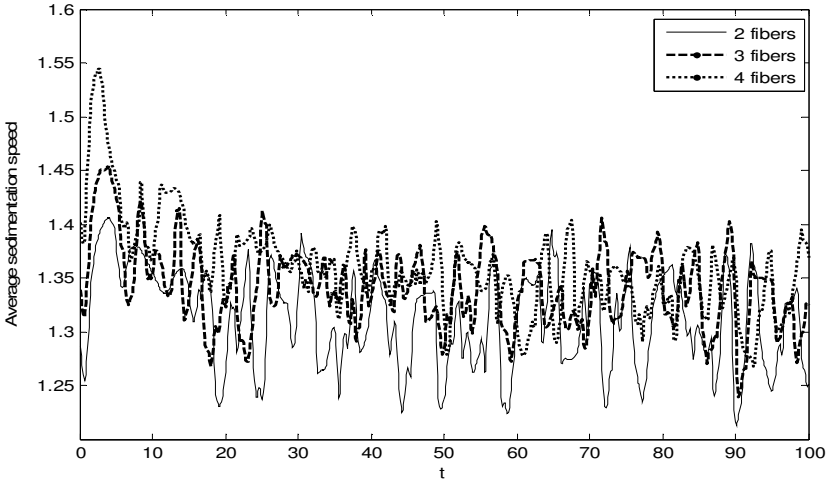

Fig. 14. Average sedimentation speed as a function of time for collections of 2,3 and 4 fibers

Next, we perform a run with two fibers; one is located above the other and having the same axis which is perpendicular to xy-plane. Let us call the upper one *fiber*-1 and the lower one *fiber*-2.

In Fig. 15, we present the configuration of fibers at four different times. Observing this figure, we see that the vertical distance between the two fibers become larger over time, which means that fiber-2 is sedimenting faster than the fiber-1.

In fact, the average sedimenting speed of fiber-2 is 1.3114 which is slightly higher than that of fiber-1 that equals 1.2884. From the trajectories of the two fibers, we can note the very different dynamic behavior of these two fibers with identical shapes.

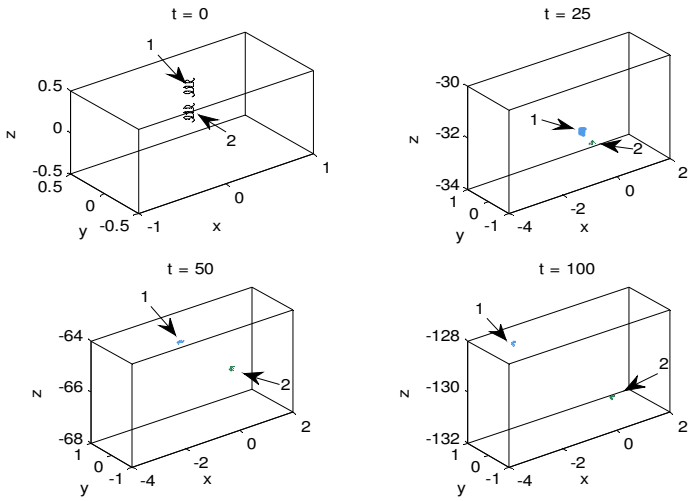

Fig. 15. Fiber configuration for 2 fibers with a vertical distribution shown at $t = 0$, $t = 25$, $t = 59$ and $t = 100$

The average sedimentation speed of the collection is shown as a function of time in Fig. 16. To study the behavior of the fibers, we picked one local bottom at $t = 50.0626$ and a local peak at $t = 52.75$. On the bottom the speed was 1.2325 whereas on the peak it was 1.3429.

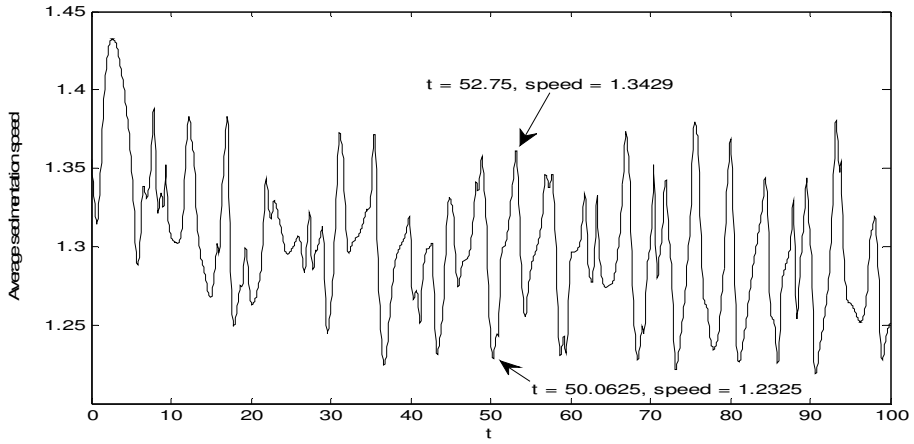

Fig. 16. Average sedimentation speed as a function of time for 2 fibers with a vertical distribution

Examining the fibers at these two times and at a point in the middle, $t = 51.375$, we found the behaviors are totally agreed with the conclusions we have gotten in single-fiber case. Separately, the sedimentation speed of single fiber increases as θ decreases.

7 Conclusions

We have developed a numerical method for the simulation of curved rigid fibers immersed in Stokes flow, based on slender body formulation, which we have applied to simulations of immersed fibers in linear shear flow and sedimentation.

The slender body theory allows us to reduce a three dimensional problem to a set of coupled one-dimensional integral equations along the fiber centerlines. The formulation is valid for Stokes flow, and contains the aspect ratio ε. The slender body equations are closed by imposing the constraints of rigid body motions.

Manipulating the equations, we obtain a linear system of equations that needs to be solved to find the translational and rotational velocities of the fiber, as well as the force distributions on each fiber. Once the velocity coefficients are known, the positions and orientations for the fibers can be updated by time-stepping separate ordinary differential equations.

We have performed simulations of single and multiple fibers in Stokes flows: shear flow and sedimentation. Results from these simulations are used to investigate different properties of the suspension such as orientation, trajectory and sedimentation speed of the fibers during the process.

It has been found that the translation and rotation of the fiber are very sensitive to the curvature. We have found that the fiber with higher curvature translating (in shear flow) and sedimenting (due to gravity) faster than the fiber with lower curvature. Moreover, the simulations have demonstrated that the curvature of a fiber affects the translation and sedimentation trajectories.

In the helix case, we have found that the sedimentation speed is well correlated with the orientation. There is a marked increase in the sedimentation speed as the angle between the helix axis and xy-plane decreases.

In order to increase the number of fibers in our simulations, there are two main improvements to be made. The first is to implement a fast summation strategy, such as is done for potential flows [25], for evaluating the Stokeslets and doublets arising from discretization of the fiber-fiber interactions. The second is to parallelize the method. This is rather straightforward as most of the computations are done on each fiber separately, and interaction terms are treated in an explicit manner.

Competing interests

Author has declared that no competing interests exist.

References

[1] Jeffery G. The motion of ellipsoidal particles immersed in a viscous fluid. Proceedings of the Royal Society A. 1922:102;161-179.

[2] Gallily I, Eisner AD. On the orderly nature of the motion of nonspherical aerosol particles. I. Deposition from a laminar flow. Journal of Colloid and Interface Science. 1979:68;320-337.

[3] Gallily I, Cohen A. On the orderly nature of the motion of nonspherical aerosol particles. II. Inertial collision between a spherical large droplet and an axially symmetrical elongated particle: Further results. Journal of Colloid and Interface Science. 1979;68:338-356.

[4] Foss JM, Frey MF, Schamberger MR, Peters JE, Leong KH. Collection of uncharged prolate spheroid particles by spherical collectors I: 2D motion. Journal of Aerosol Science. 1989;20:515-532.

[5] Chen YK, Yu CP. Sedimentation of charged fibers from a circular duct flow. Journal of Aerosol Science. 1991;23:747-756.

[6] Chwang AT. Hydromechanics of low-reynolds-number flow. Part3. Motion of a spheroidal particle in quadratic flows. Journal of Fluid Mechanics. 1975;72:17-34.

[7] Hu HH, Joseph DD, Crochet MJ. Direct simulation of fluid particle motions. Theoretical and Computational Fluid Dynamics. 1992;3:285-306.

[8] Feng J, Hu HH, Joseph DD. Direction simulation of initial value problems for the motion of solid bodies in a newtonian fluid, part2. Couette and poiseuille flows. Journal of Fluid Mechanics. 1994;277:271-301.

[9] Sugihara-Seki M. The motion of an ellipsoid in tube flow at low reynolds numbers. Journal of Fluid Mechanics. 1996;324:287-308.

[10] Zhang D, Smith DE, Jack DA, Montgomery-Smith S. Numerical evaluation of single fiber motion for short-fiber-reinforced composite materials processing. ASME Transactions Journal of Manufacturing and Science Engineering. 2011;133(5):051002-1-9.

[11] Shelley MJ, Ueda T. The Stokesian hydrodynamics of flexing, stretching filaments. Physica D: Nonlinear Phenomena. 2000;146:221–245.

[12] Qi DW. A new method of simulations of flexible particles in finite Reynolds number flows. AIChE Annual Conference, Austin, Texas; 2004.

[13] Tornberg AK, Shelley MJ. Simulating the dynamics and interaction of flexible fibers in Stokes flow. Journal of Computational Physics. 2004;196:8-40.

[14] Pozrikidis C. Boundary integral and singularity methods for viscous flow. Cambridge Press; 1992.

[15] Tornberg AK, Gustavsson K. A numerical method for simulations of rigid fiber suspensions. Journal of Computational Physics. 2006;215(1):172-196.

[16] Keller J, Rubinow S. Slender-body theory for slow viscous flow. Journal of Fluid Mechanics. 1976;75:705–714.

[17] Gotz T. Interactions of fibers and flow: Asymptotics, theory and numerics, PhD thesis, University of Kaiserslautern, Germany; 2000.

[18] Tenenbaum R. Fundamentals of Applied Dynamics. Springer; 2004.

[19] Junk M, Illner R. A new derivation of Jeffery's equation. Journal of Mathematical Fluid Mechanics. 2007;9(4):445–288.

[20] Mohapatra P, Khamari A, Raval M. A method for structural analysis of a-helices of membrane proteins. Journal of Molecular Modeling. 2004;10:393–398.

[21] Lundell F, Carlsson A. Heavy ellipsoids in creeping shear flow: transitions of the particle rotation rate and orbit shape. Physical Review E. 2010;81(1), Pt 2, 016323.

[22] Joung CG, Phan-Thien N, Fan XJ. Direct simulation of flexible fibers. Journal of Non-Newtonian Fluid Mechanics. 2001;99(1):1–36.

[23] Kahn PC. Defining the axis of a helix, Computers & Chemistry. 1989;13(3):185-189.

[24] Enkhbayar P, Damdinsuren S, Osaki M, Matsushima N. HELFIT: Helix fitting by a total least squares method. Computational Biology and Chemistry. 2008;32(4):307-310.

[25] Greengard L, Rokhlin V. A fast algorithm for particle simulations. Journal of Computational Physics. 1987;73:325-348.

Peer-review history:
The peer review history for this paper can be accessed here (Please copy paste the total link in your browser address bar)
www.sciencedomain.org/review-history.php?iid=726&id=6&aid=6659